ORIGINAL PAPER

Valorization of pyrolytic plastic-derived char for adsorption of wastewater contaminants: a kinetic and thermodynamic investigation

F. Barracco[1] · E. Parisi[1] · G. Pipitone[1] · E. Simone[1] · S. Bensaid[1] · D. Fino[1]

Abstract

The sustainable management of plastic waste is one of the challenges of our time due to the high percentage of landfilling. One of the strategies is its thermal treatment via pyrolysis, but it is associated with the production of a char, necessitating a proper valorization pathway. In this work, we investigated for the first time the use as adsorbent of a real plastic-derived char obtained as such from a pyrolysis pilot plant. This is a novel approach with respect to literature, where the char is typically obtained as desired product. The adsorbent was characterized via several techniques, and methylene blue was chosen as representative contaminant of wastewater. The inorganic component (80 wt.%) was mainly associated with the presence of rod-like structures, rich in Si, while the organic fraction showed the occurrence of aromatic components. Under the thermodynamic point of view, Langmuir isotherm effectively fitted the experimental data ($R^2 = 0.98$), while the kinetic results were well described by a pseudo-second-order law ($R^2 > 0.99$). The negative Gibbs free energy highlighted that the adsorption process was spontaneous, and the enthalpy change ($\Delta H^0 = 7.18$ kJ/mol) revealed the endothermic nature of the process, in a range characteristic of physisorption phenomena. Overall, this study highlights that a low-value char, derived from a real plastic waste, can be a promising valuable alternative to expensive adsorbents thanks to its adsorption capacity of 5.8 mg/g without prior activation treatments, hence being a starting point for the development of a holistic approach in plastic waste management.

Keywords Adsorption · Isotherms · Kinetics · Methylene blue dye · Plastic-derived char · Waste valorization

Introduction

In the last century, the use of plastic in industry has significantly increased, reaching more than 300 million tons produced every year, and becoming one of the most used materials in the world (Eriksen et al. 2020). Consequently, the sustainable management of plastic waste is a critical challenge, due to its typical short working period, accompanied by its chemical recalcitrance to natural decomposition (Chen et al. 2021). The first and most valuable strategy to solve this issue looks at the recycling of plastic. From 2006 to 2020, the amount of recycled plastic waste increased by

117% (Europe 2022), but the recycling rate is still too low, and accompanied by challenges that must be overcome due to the low bulk density and economic value, as well as issues related to the sorting machine (e.g., presence of pigments that absorb light).

Other than via mechanical recycling, plastic waste can be managed through the so-called waste-to-energy technologies (Nanda and Berruti 2021). For example, pyrolysis and gasification processes allow to produce chemicals suitable to be used as fuels or for other industrial purposes, contributing to reduce natural resource consumption according to the circular economy concept (Dogu et al. 2021).

These processes still leave behind a solid residue, known as char, which in turn can be a waste, and risks to be landfilled (Lopez et al. 2018; Antelava et al. 2021; Dogu et al. 2021). The valorization of such waste represents a further expansion of the circular economy loop of plastic waste treatment. It complies with the waste hierarchy actions defined by the European Directive 2008/98/EC (European

✉ G. Pipitone
   giuseppe.pipitone@polito.it

[1] Department of Applied Science and Technology, Politecnico di Torino, Corso Duca degli Abruzzi 24, 10129 Turin, Italy

Commission 2008), also called waste framework directive, of which the first hierarchy action applicable to char treatment is the "re-use" action. Furthermore, char valorization is also conformed to the United Nations sustainable development goals (SDG), and in particular to SDG 12, "Ensure sustainable consumption and production patterns," which states to "substantially reduce waste generation through prevention, reduction, recycling and reuse" (United Nations 2015). Biomass-derived chars have been considered sustainable alternatives to commercially available activated carbon (Dai et al. 2019); therefore, being plastic waste pyrolysis a sustainable treatment (Sharuddin et al. 2016), plastic-derived char represents a material whose valorization could contribute to developing a more sustainable society.

In recent years, several studies have been conducted to evaluate suitable alternatives for its valorization. Original works published in literature during a period ranging from 2010 to 2023 were investigated, focusing on papers regarding valorization of both biomass-derived chars and plastic-derived chars. The literature review (see paragraph 1 of supplementary materials for further details) revealed that applications of char as a fuel, in active carbon production, and as substitute for raw materials in road construction and construction industry have been investigated (Sharuddin et al. 2016). Other options involved its use as support to conduct pollutant catalytic degradation (Lai et al. 2022) and as raw material substitute for epoxy resins production (Ahmetli et al. 2013).

Another particularly interesting application has been found in using char as adsorbent media for inorganic compounds removal, thanks to char efficacy of adsorption and low cost (Godinho et al. 2017; Fuente-Cuesta et al. 2015). The application of char as adsorbent material has been extensively investigated with biomass-derived char, such in the case of heavy metals (Tan et al. 2015) and organic pollutants (Chen et al. 2017; Qu et al. 2019; Dai et al. 2019; Tan et al. 2015), and gaseous pollutants adsorption (Chen et al. 2017). On the other hand, chars derived from plastic wastes pyrolysis, particularly referring to solely plastic waste char, were not as widely studied, either for inorganic pollutants (Martín-Lara et al. 2021; Singh et al. 2020) or organic pollutants removal (Li et al. 2021; Mun et al. 2022).

In most of the reviewed papers, alongside investigating the adsorption performance, a study of the adsorption kinetics and isotherm adsorption was conducted. Moreover, some papers also investigated the thermodynamic aspects of the adsorption (Qu et al. 2019; Hoslett et al. 2019; Essawy et al. 2017; Singh et al. 2020). Also, all the already cited papers displayed some characterization techniques aimed to provide further information on the adsorption process.

Furthermore, to determine whether the investigated chars could already be useful from an industrial point of view without further treatment, some of the reviewed studies compared the investigated chars with commercially available activated carbons, observing different outcomes. Regarding wastewater treatment, some chars achieved similar or even higher adsorption performances to those of commercial activated carbons, whereas others showed lower efficacy. In particular, Hoslett et al. observed that non-activated chars derived from municipal solid waste pyrolysis achieved an adsorption performance significantly lower than that of commercially available activated carbon (Hoslett et al. 2020; 2019); on the other hand, Li et al. observed that polyurethane-derived activated char possessed higher sorbent capacities than commercial activated carbons (Li et al. 2021). This observation from other studies seems to suggest char activation to potentially be a key element in emulating the efficacy of commercially available activated carbons. Despite activation represents a non-negligible cost, it could lead to a sorbent superior to already commercialized carbons, as showed by Li et al. and, at the same time, offer an alternative to the disposal of chars.

It is worthy to note that most of the work conducted so far involved char in co-pyrolysis, or co-gasification, of plastic waste and other materials, such as biomasses (Xu et al. 2019; Godinho et al. 2017), municipal solid waste (Hoslett et al. 2019), waste paper (Fuente-Cuesta et al. 2015), or various blends (Ahmed and Hameed 2020), thus showing a limited amount of studies on sole plastic waste char. Furthermore, these studies involved the use of a plastic waste feedstock composed by just one type of plastic polymer (Li et al. 2021; Essawy et al. 2017; Mun et al. 2022). Finally, to the authors' knowledge, char was usually the desired product of the process conducted for the study, and it was often limited to the laboratory scale (Li et al. 2021; Mun et al. 2022; Martín-Lara et al. 2021; Essawy et al. 2017; Hoslett et al. 2019). However, plastic waste is usually composed by several different types of polymers, such as the case of packaging waste (Dahlbo et al. 2018), resulting in a heterogeneous polymer mixture, especially in the case of municipal plastic waste (Zhang et al. 2020). Thus, the behavior of chars obtained from a single-polymer feedstock may not be representative of the real waste. In addition, the characteristics of chars obtained as the desired product of the laboratory-scale process might not be similar to the ones obtained as residual waste of industrial processes.

In order to fill this gap, the char analyzed in this work was obtained as an actual by-product of a pyrolysis process at pilot scale, under operative conditions not optimized for its production: this resulted in a novel approach toward char studies as adsorbent media, since it provides information on the performance of a real waste in the very first valorization stage. The feed of the pyrolysis plant was mainly composed of plastic packaging and scrap plastic from out of use vehicles dismantlement.

The obtained char was studied for the adsorption of methylene blue (MB), an industrially used dye whose removal from wastewaters has been extensively investigated through years due to risks posed to human health (Santoso et al. 2020). The char was extensively characterized through different techniques (thermal degradation, field emission scanning electron microscopy, energy dispersive X-ray analysis, Fourier transform infrared spectroscopy, X-ray diffraction, Raman spectroscopy, N_2 adsorption–desorption) to get insights on its organic and inorganic matter content, morphological, structural, textural, bulk, and superficial properties. The objective of this work was to investigate the sorbent properties of a char obtained as residual waste of a real pilot-scale pyrolysis process; thus, the influence of temperature and MB initial concentration on the percentage removal and char adsorption capacity was investigated. In addition, the adsorption kinetics and isotherms were evaluated, alongside the adsorption mechanism and mass transfer phenomena influence on adsorption.

Overall, this work allowed to increase our understanding on the valorization pathways of real multi-polymer-plastic-derived char, contributing to the development of sustainable waste management practices and the creation of a circular economy.

Materials and methods

Materials

Plastic waste char (PW-C) was obtained from Benzi and Partners S.r.l. pilot plant. The pyrolyzed plastic waste was composed by plastic packaging and plastic scrap from dismantled vehicles. Similarly to what is reported in the literature, the mixed plastic waste contained, among other polymers, polypropylene (PP), polyethylene (PE), and acrylonitrile butadiene styrene (ABS) (Roosen et al. 2020; Cossu et al. 2014).

The mixed plastic waste was pyrolyzed at 650 °C in an electric-heated rotary kiln, obtaining PW-C as solid residue. The PW-C was then manually grinded, to obtain a more uniform dimension of the particles, and no other pre-treatment was effectuated. Methylene blue (≥ 97% mass purity) was purchased from Merck and used without further purification. Distilled water was utilized for methylene blue solution preparation. It was produced in the laboratory thanks to a purification system consisting of a low-pressure reverse osmosis and ion exchange resins.

Char characterization

A series of analyses were conducted to characterize the char.

Thermal degradation tests were performed on PW-C, to assess its organic compounds content. PW-C was calcinated at a temperature of 850 °C, under air atmosphere. The calcination temperature was maintained for a duration of 1 h. To assess the content of humidity lost during the thermal degradation, PW-C was also desiccated at 105 °C for 24 h.

Field emission scanning electron microscopy (FE-SEM) was employed to investigate PW-C morphology. FE-SEM was conducted with electron high tension (EHT) = 5 kV and magnification ranging from $100\times$ to $10^4\times$. Energy dispersive X-ray (EDX) was also used to determine the elements present in PW-C (Hoslett et al. 2019).

Fourier transform infrared (FT-IR) spectroscopy analysis was conducted on the fresh sample (Bruker Tensor 27 FT-IR spectrophotometer) to investigate the presence of functional groups in PW-C structure. In addition, it was conducted on spent samples (i.e., after the adsorption test) to investigate the new bonds formed with the adsorbed MB and the adsorption mechanism of MB onto PW-C surface.

XRD analysis was carried out to investigate the possible crystalline nature of the sample, with a degree interval between 10° and 90°, 0.013° step size, and 240 s per step. The degree interval was chosen in accordance with other characterizations of plastic-derived chars (Singh et al. 2020; Essawy et al. 2017; Godinho et al. 2017).

Raman spectroscopy was used to determine the presence of graphitic ordered and disordered structures in the char (Li et al. 2021; Essawy et al. 2017). All Raman spectra were obtained at room temperature (298 K) using a Horiba LabRAM HR Evolution spectrometer. The instrument is equipped with a multicanal CCD UV (1024×256 pixels) detector, 1800R/mm high-resolution grating, and 532-nm laser was used as excitation source to deliver a laser power of 25 mW. The char sample was measured with a $50\times$ UV LWD confocal volume Olympus objective. Every measurement was collected using 10 s of acquisition time and 60 accumulations (Ko et al. 2021; Essawy et al. 2017). The presence of graphitic ordered and disordered structures was estimated using the I_D/I_G area ratio, which refers to the D and G bands, originated from defective graphitic structures and graphitic sp^2 bonds, respectively (Ferrari and Robertson 2000). The Raman spectroscopy was performed in an interval extending from 120 to 2000 cm^{-1}, focusing on the 1250–1650 cm^{-1} range, to capture the region where D and G bands are usually observed in (1300–1610 cm^{-1}) (Ferrari and Robertson 2000; Ko et al. 2021). The Raman spectra were then smoothened, and the baseline was subtracted to eliminate background signals. The spectra were then analyzed to obtain the D and G bands area I_D and I_G, calculating the integral area of the bands. To calculate the bands area, Origin 2018 software "integrate peaks" function was used.

Lastly, to assess the surface area, nitrogen adsorption–desorption isotherms were obtained in a Micromeritics

Tristar 3020 set up. Brunauer–Emmett–Teller (BET) method was performed on PW-C, while pore volume and pore width were assessed through Barrett–Joyner–Halenda (BJH) method. Before conducting the surface area analysis, the sample was pre-treated by heating and maintaining the sample at 200 °C for 2 h, to remove humidity from the char surface.

Adsorption tests description

Each test was prepared starting from a 200 mg/L methylene blue stock aqueous solution. The analyzed initial MB concentrations were 20 mg/L, 40 mg/L, 60 mg/L, 80 mg/L, and 100 mg/L, in accordance with similar previous works (Achari et al. 2021; Baloo et al. 2021).

The influence of solid adsorbent amount and initial MB concentration influence was analyzed varying one parameter at a time. Therefore, to investigate char mass influence, the tests were conducted using a 20 mg/L MB solution and char mass dosages of 0.5 g, 1 g, 1.5 g, 2 g, and 2.5 g, while to assess initial MB concentration influence, MB concentration ranged from 20 to 100 mg/L, keeping char dosage constant at 2 g. To ensure the same fluid dynamics regime occurred between experiments, every test was conducted using a volume of MB solution equal to 200 ml. Each test was conducted in duplicates.

Once prepared the MB solution, PW-C was first manually grinded using a mortar and pestle to obtain a more uniform dimension of the char particles. Prior to starting the tests, a sample of the initial MB solution was taken to have a reference absorbance value for the initial MB concentration. To assess the adsorption performance, UV–visible spectrophotometry at 664 nm was utilized, using Hach Lange DR 5000 spectrophotometer. Afterward, PW-C was added to the solution and the stirring was started. The tests were conducted at 300 rpm, identified as optimal agitation speed through

preliminary tests (Figure S1, Supplementary Information), and lasted for a total of contact time of 360 min.

During the test duration, the solution was periodically sampled. To assess the adsorption performance, MB relative removal (Eq. (1)), expressed as a percentage, and PW-C adsorption capacity (Eq. (2)), expressed in mg of MB adsorbed per gram of char, were evaluated.

$$\text{Removal}_t(\%) = \frac{C_0 V_0 - C_t V_t}{C_0 \cdot V_0} \cdot 100 \quad (1)$$

$$q_t(\text{mg/g}) = \frac{C_0 V_0 - C_t V_t}{m_{\text{char}}} \quad (2)$$

In Eqs. (1) and (2), C_0 represents the initial MB concentration (mg/L), V_0 represents the solution initial volume (L), C_t and V_t represents the bulk solution MB concentration (mg/L) and solution volume (L), respectively, at a given time instant. In Eq. (2), m_{char} represents the char dosage (g) used to conduct the adsorption.

A visual representation of the adsorption tests preparation and performing is provided in Fig. 1.

Adsorption thermodynamic and kinetic studies

Adsorption isotherm study

To assess the adsorption phenomena, two types of mechanism were examined, namely Langmuir and Freundlich isotherms (Fu et al. 2015; Li et al. 2021). Dubinin–Radushkevich (D–R) isotherm fitting of the data was also studied, but the results are not reported here because of the poor data fitting (more information in the supplementary material).

Langmuir isotherm, reported in Eq. (3), assumes the formation of a sorbate monolayer on homogeneous active sites, with no interaction between adsorbed molecules. As
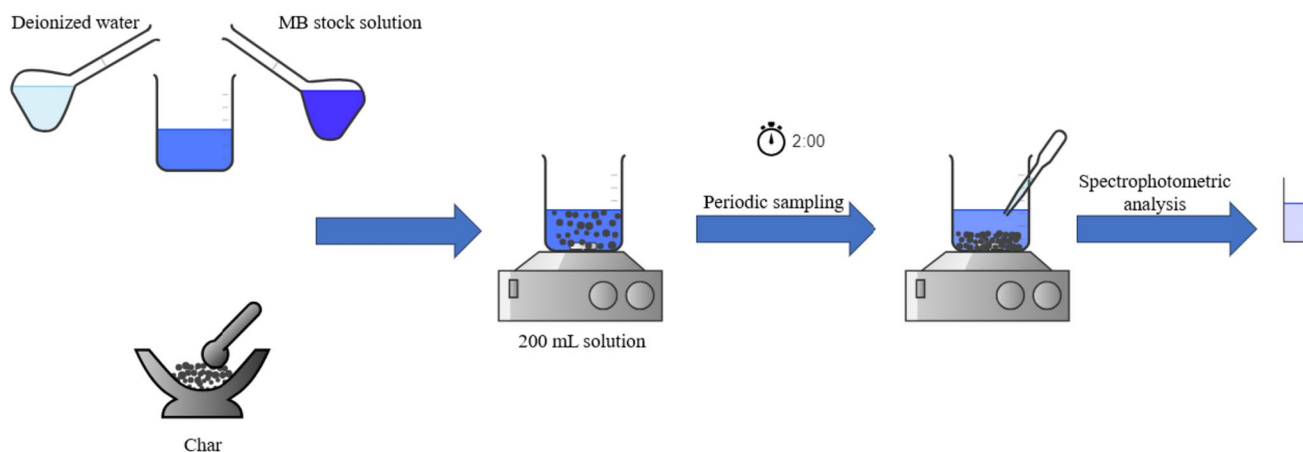

Fig. 1 Flowchart of conducted adsorption tests in this work

a result, the enthalpy of adsorption is constant through the entire adsorption surface and sites.

$$\frac{C_{eq}}{q_{eq}} = \frac{1}{q_m \cdot K_L} + \frac{C_{eq}}{q_m} \tag{3}$$

In Eq. (3), C_{eq} represents the MB bulk concentration at equilibrium (mg/L), q_{eq} is the mass of MB adsorbed at equilibrium over PW-C dose (mg/g), q_m is the theoretical maximum MB mass adsorbed as a monolayer over PW-C dose (mg/g), and K_L is the Langmuir isotherm constant (L/mg). In cases of processes described by Langmuir isotherm, a separation factor can be defined (Eq. (4))

$$R_L = \frac{1}{1 + K_L \cdot C_0} \tag{4}$$

In Eq. (4), C_0 represents the initial adsorbate concentration. A R_L value equal to 1 means a linear adsorption, whereas $R_L = 0$ indicates an irreversible adsorption. When $0 < R_L < 1$, the adsorption is favorable, whereas $R_L > 1$ means a non-favorable adsorption (Essawy et al. 2017; Fu et al. 2015).

The Freundlich isotherm, on the other hand, assumes a multilayer adsorption on a heterogeneous surface, resulting in adsorption enthalpy not being constant through the adsorption surface and sites.

$$\ln q_{eq} = \ln K_F + \frac{\ln C_{eq}}{n} \tag{5}$$

In Eq. (5), C_{eq} represents the MB bulk concentration at equilibrium (mg/L), q_{eq} is the mass of MB adsorbed at equilibrium over PW-C dose (mg/g), K_F represents the Freundlich isotherm constant (L/mg), and n is a parameter related to adsorption intensity.

Adsorption kinetics study

To determine the kinetic parameters describing the MB adsorption, three different models were evaluated, namely the Langergren pseudo-first-order model, the Ho and McKay pseudo-second-order model, and the intra-particle diffusion model. The corresponding linearized equations of the kinetic models are reported in Eqs. (6), (7) and (8), respectively (Li et al. 2021).

The study of adsorption kinetics was finalized to provide a better understanding of the MB adsorption process and the char suitability as a wastewater pollutants sorbent. Moreover, the model provided by kinetic studies can be useful for designing the adsorption process when integrating the sorbent char in a real process, as also stated in the literature (Fuente-Cuesta et al. 2015).

Langergren pseudo-first-order (PFO) model assumes that the rate of adsorption is dependent on the difference between the mass of adsorbed solute at the equilibrium and the mass of adsorbed solute at the considered time instant (Sahoo and Prelot 2020). Moreover, the pseudo-first-order model assumes that only one mechanism acts on the available sorption sites (Essawy et al. 2017).

$$\ln(q_{eq} - q_t) = \ln q_{eq} - k_I \cdot t \tag{6}$$

In Eq. (6), t is the contact time (min), q_t represents the adsorbed mass of MB over PW-C dose (mg/g), k_I is the pseudo-first-order rate constant (1/min), and q_{eq} is the maximum mass of MB adsorbed at equilibrium over PW-C dose (mg/g).

The Ho and McKay pseudo-second-order (PSO) model is based on the assumptions that the adsorption significantly contributes to the kinetic rate-limiting step and that the adsorption capacity is proportional to the number of occupied and unoccupied active sites on the sorbent surface (Ho and McKay 1999).

$$\frac{t}{q_t} = \frac{t}{q_{eq}} + \frac{1}{k_{II} \cdot q_{eq}^2} \tag{7}$$

In Eq. (7), k_{II} is the pseudo-second-order rate constant (g/(mg min)).

When designing a char adsorption operation for a real process, the best-fitting kinetic model could provide useful information to optimize the residence time of the wastewater through the layer of sorbent char, predicting the maximum working time before reaching q_t equilibrium values.

In several literature works, the linearized intra-particle diffusion model allowed to determine whether, other than the chemisorption or physisorption step, the external film diffusion or intra-particle diffusion contributed to the global adsorption process rate-determining steps (Fan et al. 2017; Li et al. 2021).

$$q_t = k_P \cdot t^{1/2} + C \tag{8}$$

In Eq. (8), k_p is the intra-particle adsorption rate constant (mg/(g min$^{1/2}$)) and C is a constant (mg/g) used to determine the effect of external film diffusion on the global adsorption kinetics. For $C = 0$, intra-particle diffusion limits the adsorption process, while for values different than zero, external film diffusion plays a role in limiting the adsorption process. In this case, a multilinearity of the model could be present for different time ranges. Usually, the first linear section of the model indicates external diffusion being the rate-determining step in that timeframe, whereas the second linear section indicates intra-particle diffusion as rate-determining step. Thus, multilinearity could suggest both external diffusion and intra-particle diffusion as contributing phenomena

to the rate-determining steps (Chen and Bai 2013; Li et al. 2021).

In conjunction with Eq. (8), it can be useful to employ also the Boyd model, reported in Eqs. (9), (10) and (11) (Travália and Forte 2020a, b).

$$F = \frac{q_t}{q_{eq}} \tag{9}$$

$$\text{For } F < 0.85 \ B_t = \pi \cdot \left(1 - \sqrt{1 - \frac{\pi}{3}F}\right)^2 \tag{10}$$

$$\text{For } F > 0.85 \ B_t = -0.4977 - \ln(1 - F) \tag{11}$$

In Eq. (9), F is a fraction of the mass of MB adsorbable at equilibrium. B_t represents a parameter which can be determined as a function of F, as reported in Eqs. (10) and (11), and dependent on the solute diffusivity coefficient inside the pores, on the radius of the sorbent particles, and on the time of adsorption (Boyd et al. 1947).

In a similar way to intra-particle diffusion model, the B_t vs t plot intercept allows to determine the influence of external and internal diffusion on the process kinetics. When the B_t vs t line intercepts at the origin, internal diffusion represents the rate-limiting step. In other cases, both internal diffusion and external diffusion play a role in determining the process kinetics, with external diffusion being the slowest phenomenon over the course of the entire adsorption process (Travália and Forte 2020a, b; Vadivelan and Kumar 2005).

Eqs (8) to (11) can provide useful information regarding the kinetic regime of the adsorption process. By identifying the kinetically controlling mass transfer phenomenon, the adsorption can be further optimized. For example, in case of limiting external mass transfer, it can be improved by increasing the Reynolds number.

Enthalpy and Gibbs free energy study

Thermodynamic parameters were calculated using Van't Hoff equations, represented in Eqs. (12) and (13).

$$\Delta G^0 = -RT \ln K \tag{12}$$

$$\ln K = \frac{\Delta S^0}{R} - \frac{\Delta H^0}{RT} \tag{13}$$

where K is a dimensionless equilibrium value derived from the Langmuir isotherm constant (Tomul et al. 2020) and expressed in Eq. (14), ΔG^0 symbolizes the standard Gibbs free energy, R is the universal gas constant (8.314 J/(mol K)), ΔS^0 the standard entropy, and ΔH^0 symbolizes the adsorption standard enthalpy.

$$K = K_L \cdot MM_{MB} \cdot C^0 \cdot 1000 \ mg/g \tag{14}$$

In Eq. (14), MM_{MB} represents the MB molar mass (g/mol), and C^0 represents the standard state molar concentration (1 mol/L).

To determine the value of K at different temperatures, a series of experiments were conducted, at 35, 45, and 55 °C, in addition to the experiments conducted at 20 °C. Each of the temperature tests was conducted using 2 g of PW-C, starting solution volume of 200 ml and stirred at 300 rpm. The initial MB concentration was varied between 20, 40, 60, and 80 mg/L.

Results and discussion

Char characterization

The PW-C was subjected to several analysis to assess its properties.

An average 20.5% dry-basis mass loss followed PW-C degradation tests, identifying PW-C as a mainly inorganic char. The relatively low organic matter content can be explained accounting the pyrolysis feedstock and operative conditions. As observed by several authors, the higher the pyrolysis temperature, the lower the organic matter content (Harussani et al. 2021; Martín-Lara et al. 2021). As a matter of fact, PW-C was obtained at 650 °C temperature, higher than most plastic compounds decomposition temperature (Hoslett et al. 2019), leading to most of the organic content degrading during the pyrolysis, in line with similar mass loss reported in literature (Martín-Lara et al. 2021).

FE-SEM (Fig. 2A) revealed PW-C to be largely heterogeneous. Particularly, the presence of several rod structures was noticed, all characterized by roughly the same diameter (~ 11 μm), other than the rest of the char particles matrix. Notably, the rods constituted a significant fraction of the char surface, hence likely playing a significant role in the adsorption mechanism. The largely heterogeneous morphology of the char could be attributed both to different types of pyrolyzed plastics and to the possible metal parts present, due to the plastic waste deriving mainly from vehicle scraps. Further FE-SEM images and maps are available in Supplementary Information (Fig. S2).

PW-C heterogeneity was further confirmed by EDX results (Table S1, supplementary materials). EDX analyzed the rod parts of PW-C and two different spots of the char matrix. The char matrix composition was observed to differ based on the actual part of the matrix, displaying quite different content extents of the detected elements. Nonetheless, the same elements were detected in the two matrix parts. On the contrary, the rod parts differed both in content and detected elements, containing more silicon than carbon

Fig. 2 PW-C characteriza-
tion results. **A** FE-SEM image
of PW-C. The rods dimen-
sions relative to the rest of
PW-C and their presence are
clearly visible. Magnification
1000x; **B** representation of
PW-C "rod," "crystalline," and
"carbonaceous" parts sub-
jected to Raman spectroscopy.
Magnification 5000x; **C** PW-C
upper surface map. The clearer
portions represent lower-height
zones. A depression in cor-
responding to a rod is visible: **D**
FT-IR analysis of PW-C prior
to and post-MB adsorption. MB
adsorption was conducted at
80 mg/L initial MB concentra-
tion. **E** PW-C XRD analysis
spectrum. Most detected
compounds were indicated
through a symbol above the
corresponding peaks. Graphitic
structures were the only excep-
tion, being indicated through a
symbol placed underneath the
corresponding band. The rest
of the peaks are identified in
Section "Char characterization"
text. Ψ: graphitic structures;
♠ = Mg_3SiO_4; ♣ = TiO_2;
♥ = SiO_2; ♦ = $CaCO_3$. **F** F
Raman spectra of PW-C in the
1250–1650 cm^{-1} range. The
detected *D*, *G*, and amorphous
bands were represented, along
with an indicative position of
their peaks
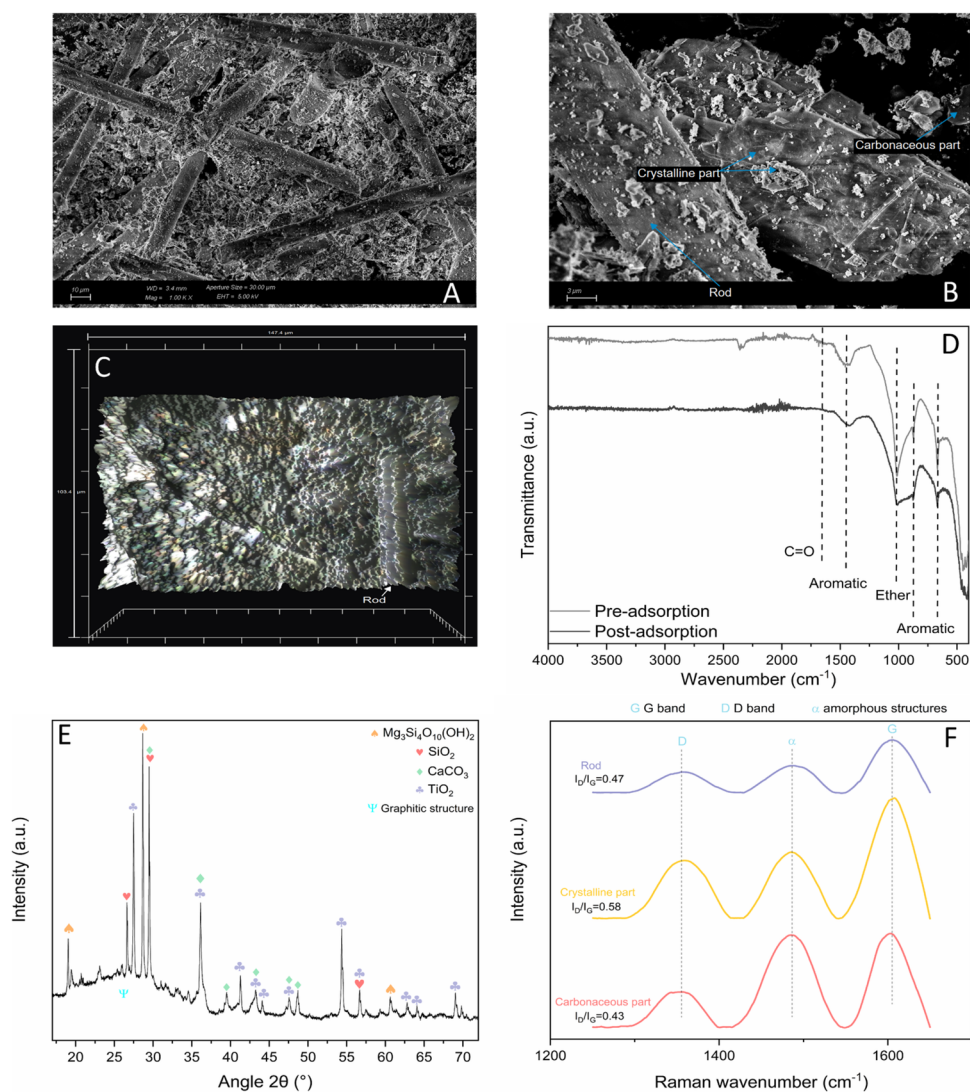
(~ 19.6% and ~ 7.88% of detected atoms, respectively). Fur-
thermore, aluminum and calcium were detected in appreci-
able quantity in the rods, while only being present in traces
in the char matrix. Thus, the rod parts probably derived from
the metals present in the vehicle scrap plastics. PW-C was
hence showed to be peculiar, due to the rods presence, which
might have played an impactful role in MB adsorption and
whose topography was shown in a map (Fig. 2C).

FT-IR spectroscopy was conducted on fresh and spent
PW-C. Before the adsorption (Fig. 2D), several signals
between roughly 2350 and 400 cm^{-1} could be identified. The
1600–1660 cm^{-1} shoulder might be linked to a relatively low
presence of carboxylic groups and ester C=O bonds (Lai
et al. 2022; Essawy et al. 2017). The band between 1500 and
1250 cm^{-1} and the peaks at approximately 870 and 650 cm^{-1}
indicated the presence of aromatic compounds, more specifi-
cally phenyl groups (1500–1250 cm^{-1}; 870 cm^{-1}) (Li et al.
2021) and aromatic C–H bonds (870 cm^{-1}; 650 cm^{-1}) (Mun
et al. 2022; Li et al. 2021). The band between roughly 500

and 400 cm^{-1} identified Si–O–Si bonds (Fan et al. 2017).
The 1050-cm^{-1} peak could suggest the presence of ether
C–O and C–O–C bonds (Fan et al. 2017; Lai et al. 2022),
which would be supported by the peak extending its signal
up to approximately 1200 cm^{-1}, due to signals between 1300
and 1100 cm^{-1} identifying presence of ether groups (Mun
et al. 2022; Li et al. 2021). At approximately 2350 cm^{-1}, a
signal may indicate a CC alkyne triple bond (Li et al. 2016).

Due to low adsorbed MB mass, the post-adsorption spec-
trum did not show most of MB characteristic signals, similar
to what was observed by Obeso et al. 2022. Nevertheless,
spent PW-C char FT-IR functional groups were modified by
MB adsorption.

After the dye adsorption, the band between 1500 and
1250 cm^{-1} was slightly shifted toward lower frequencies,
and both the 1500–1250 cm^{-1} band and 640 cm^{-1} peak
intensity were relatively reduced, signifying an involvement
of PW-C aromatic compounds in the adsorption, possibly
through π bonds interactions (Ovchinnikov et al. 2016; Fu

et al. 2015). More importantly, between 1050 and 850 cm^{-1} a new band was registered, suggesting the possible involvement of MB sulfur atoms in the adsorption, and the presence of hydrogen bonds between PW-C surface and MB molecules nitrogen atoms, as stated by Ovchinnikov et al. 2016. At 500–400 cm^{-1}, the band was slightly shifted and widened toward lower frequencies, possibly signifying a degree of interaction of Si–O–Si bonds in MB adsorption (Fan et al. 2017). Finally, the absence of shoulder at 1660–1600 cm^{-1} might indicate carboxyl COOH groups interacting with MB.

Thus, the observed differences between pre- and post-adsorption FT-IR analyses determined the importance of MB aromatic characteristics and heteroatoms (nitrogen and sulfur) presence and were used to investigate possible adsorption mechanisms, of which a more detailed account is given in "Adsorption Mechanism" section.

The XRD (Fig. 2E) was characterized by several peaks that could be associated with different mineral oxides. Among the peaks, silica presence was suggested by peaks at degrees $2\theta = 26.6°$, 29.5°, and 56.6° (Tomul et al. 2020; Zhang et al. 2020; Godinho et al. 2017). These findings agreed with EDX results, which showed Si to be among the most present elements (even higher than carbon in rods), and with FT-IR spectroscopy, which revealed the presence of Si–O–Si bonds. Other than SiO$_2$, CaCO$_3$ presence was revealed by the diffractogram peaks at degrees $2\theta = 29.5°$, 36.3°, 39.5° (Tomul et al. 2020), 43.3°, 47.6°, and 48°, likely explained by the calcium present in the rods (Table S1, Supplementary Material). Titanium was also likely largely present in the diffractogram as TiO$_2$, being suggested by peaks at $2\theta = 27.4°$, 36.3°, 41.2°, 43.3°, 44°, 47.6°, 64° (Singh et al. 2020; Godinho et al. 2017), 54.5°, 56.6°, 62.9°, and 69°. TiO$_2$ presence might be explained by its use as plastic pigment (Singh et al. 2020). Moreover, the band at 26° and the surrounding region might be linked to graphitic structures (Li et al. 2021; Lai et al. 2022), more specifically detecting imperfect graphitic structures (Sergiienko et al. 2009). Interestingly, magnesium silicate hydroxide was detected at $2\theta = 19°$, 28.6°, and 60.9° (Perdikatsis and Burzlaff 1981), meaning that not all the detected silicon belonged to SiO$_2$ structures.

Raman spectroscopy (Figs. 2F, S3) was performed to determine the grade of graphitization of PW-C and to further investigate the presence of inorganic compounds in the char. Three spots of PW-C were analyzed, namely the rods and two different sites of PW-C matrix, denominated "carbonaceous" and "crystalline" parts, based only on visual criteria. For a better understanding and distinction of the analyzed PW-C parts, the three spots are identified in Fig. 2B. Silica (SiO$_2$) was detected in all the three parts of PW-C, with the signal's intensity changing based on the part of PW-C under analysis. Ca$_2$SiO$_4$ was also detected, again suggesting that the Si–O-Si bonds reported by FT-IR were not entirely

correlated with silica. TiO$_2$ and possibly Al$_2$O$_3$ were also spotted, confirming EDX. Regarding the carbon structures, the presence of carbonyl C=O groups, confirming the FT-IR analysis findings, and C=C bonds was revealed. Other than that, every analyzed PW-C part showed D and G bands, each peaking at 1350–1365 cm^{-1} and at 1597–1603 cm^{-1} wavenumber, respectively. These two bands contain valuable information regarding the graphitic degree of the char structure (Sergiienko et al. 2009; Ferrari and Robertson 2000). The D band is the signal caused by graphitic breathing vibrational mode, occurring only in non-perfect graphitic crystals, supporting the presence of the imperfect graphitic structure detected by the XRD, while the G band originates from sp^2 bonds stretching in both perfect and non-perfect graphites (Ferrari and Robertson 2000), despite D and G bands also corresponding to signals tied to aromatic compounds presence (Ferrari and Robertson 2000; Ko et al. 2021). The analyzed PW-C parts showed a I$_D$/I$_G$ ratio equal to 0.43 in the "carbonaceous" PW-C matrix part, 0.58 in the crystalline PW-C matrix part, and 0.47 in the rods. Thus, PW-C was characterized by few defective graphitic structures. However, as represented in Fig. 2F, the amorphous carbon band, located around 1480–1500 cm^{-1} (Ko et al. 2021), was fairly intense for all PW-C parts, especially in the "carbonaceous" matrix part. Thus, PW-C may be characterized by a non-negligible quantity of amorphous carbon structures. While defective graphite maintains a prevalently sp^2 hybridization, amorphous carbons present vastly different characteristics. (Ferrari and Robertson 2000). In Supplementary Materials, PW-C carbon structures were further investigated.

Lastly, N$_2$ adsorption–desorption tests resulted in an average BET surface area of 13.6 m^2/g, an average BJH pore volume of 0.0298 cm^3/g, and BJH pore width of 18.9 nm, identifying the PW-C as a mainly mesoporous char, as observed for other plastic-derived chars (Singh et al. 2021; Miandad et al. 2018). Despite the measured BET surface being relatively low, when compared to activated chars or biochars BET surfaces (El-Shafey et al. 2016; Hassan et al. 2014), other literature works reported similar BET surfaces for plastic-derived chars and biochars (Santoso et al. 2020; Singh et al. 2021). The relatively low BET surface could be explained by the low pore volume, when compared to values reported in the literature (Hassan et al. 2014; Mun et al. 2022), and the mesoporous nature of the pores.

PW-C adsorption performance

Figure 3 illustrates the influence of initial MB concentration and PW-C dose on MB removal and adsorption capacity over time.

In Fig 3- A, keeping constant the initial MB concentration at 20 mg/L, it was observed that increasing PW-C dose led to an increase in MB relative removal, ranging
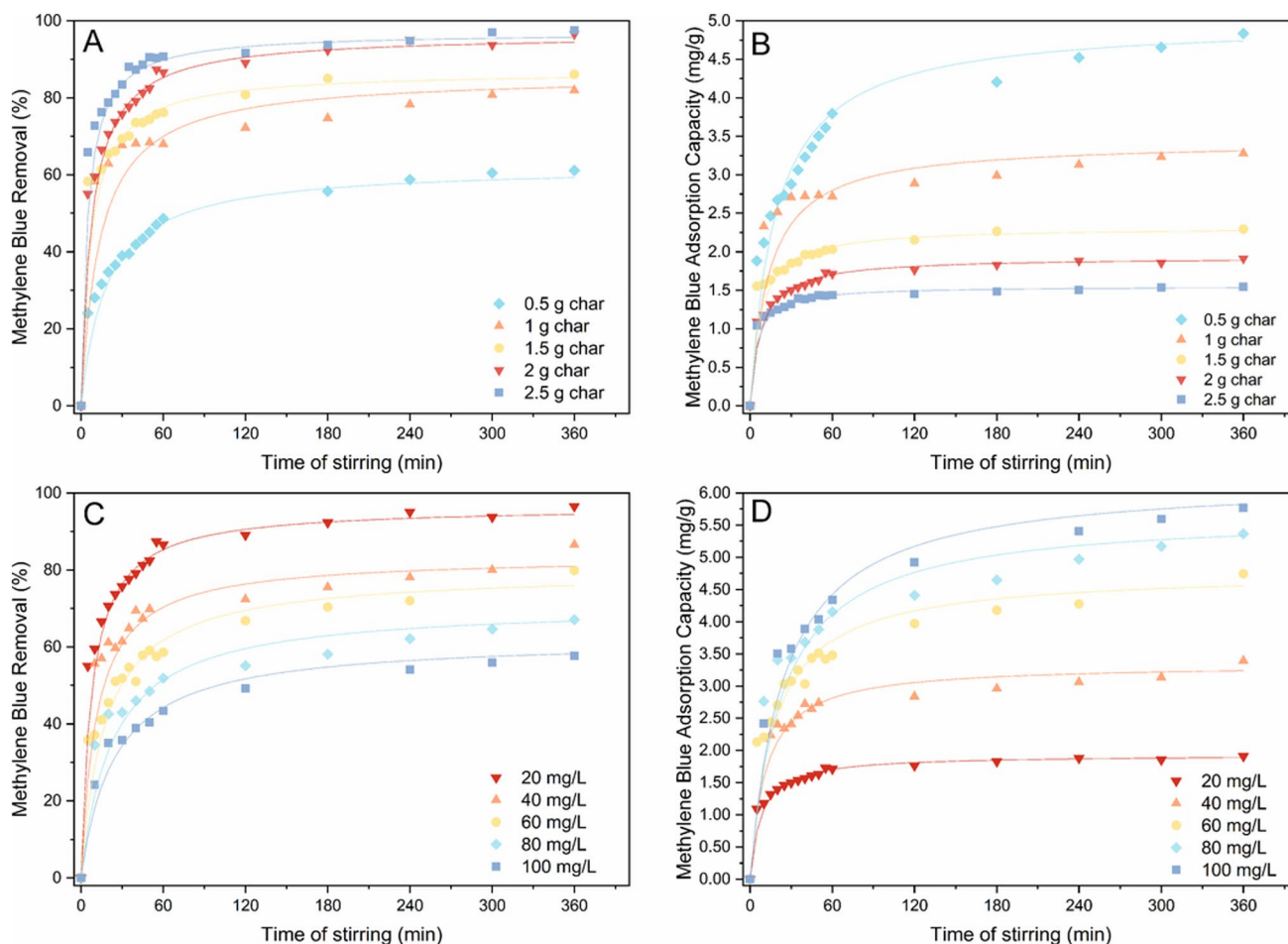
Fig. 3 Influence of initial MB concentration, and PW-C dose on MB adsorption over time. **a** Influence of PW-C dose on MB removal, at 20 mg/L initial MB concentration; **b** influence of PW-C dose on MB adsorption capacity, at 20 mg/L initial MB concentration; **c** influence of initial MB concentration on MB removal, at 2 g PW-C dose; **d** influence of initial MB concentration on MB adsorption capacity, at 2 g PW-C dose. All data were collected at room temperature

from 58% to about 97% at maximum dosage, in accordance with the literature (Mun et al. 2022; Singh et al. 2020). On the other hand, as shown in Fig. 3B, increasing the PW-C dosage led to a decrease in MB adsorption capacity from roughly 4.8 mg/g at minimum dose to about 1.5 mg/g, as also observed by Fan et al. 2017. Increasing PW-C amount resulted in a higher number of available adsorption sites, which promoted the MB uptake; nevertheless, this phenomenon is not linear, causing a decrease in the adsorption capacity. A possible explanation could be attributed to a temporal and partial agglomeration of char particles during the adsorption process (Ngueagni et al. 2021; Tran et al. 2022), partially hindering MB molecules access to a part of the pores and adsorption sites of PW-C. The coverage degree may have hence varied non-linearly with the increase in PW-C dosage, leading to the observed behavior. A similar effect was observed for saturated char, where

increasing char dosage did not lead to an increase in MB removal (Wu et al. 2022; Joshiba et al. 2022).

Regarding the influence of initial MB concentration, Fig. 3C illustrates how, at a fixed 2 g PW-C dosage, increasing initial MB concentration led to decreasing relative removal from 96 to about 60% at maximum MB concentration, a trend agreeing with the literature (Dao et al. 2021; Essawy et al. 2017). Simultaneously, an increase in initial MB concentration led to an increase in adsorption capacity, from 1.9 to 5.8 mg/g at 100 mg/L MB concentration, as shown in Fig. 3D. A similar trend was observed by Li et al. 2021 and Fu et al. 2015. Increasing initial MB concentration led to increasing the adsorbed MB mass at equilibrium, due to the higher concentration gradient between bulk and char surface, and hence a higher driving force.

Compared to some other chars tested in literature for adsorption of pollutant dyes (Table 1), PW-C showed

Table 1 Comparison of char capacity adsorption of MB and other dyes and aromatic compounds. The adsorption capacity value reported for this work was obtained from data deriving from adsorption on 2 g of char at 20 °C

Char feedstock	Activated char	Sorbate	Sorbate initial concentration (mg/L)	Adsorption capacity (mg/g)	Reference
Mixed plastic waste	No	MB	100	5.80	This work
Mixed plastic waste	No	MB	20	1.90	This work
Pine wood	No	MB	100	~2.4	Lonappan et al. 2016
Pig manure	No	MB	100	10.0	Lonappan et al. 2016
Paper	No	MB	100	~7.4	Lonappan et al. 2016
Palm bark	No	MB	15	1.2	Sun et al. 2013
Digestate residue	No	MB	15	1.7	Sun et al. 2013
Paper and pulp sludge	No	Methyl orange (MO)	100	~11.0	Chaukura et al. 2017
Coconut coir dust	Yes	MB	3	~13.8	Souza et al. 2006
Eggshell membrane	Yes	MB	22	110.4	Wu et al. 2022
Mixed plastic waste	Yes	Color in paper and pulp milling wastewaters	65	~12.0	Gupta et al. 2022
Mixed municipal discarded material	No	MB	100	7.2	Hoslett et al. 2020
Polyurethane plastic waste	Yes	Malachite green (MG)	100	250.0	Li et al. 2021)
Coconut †	Yes	MG	200	83.1	Qu et al. 2019
Coal †	Yes	MG	200	74.9	Qu et al. 2019
Apricot †	Yes	MG	200	69.6	Qu et al. 2019
Peach †	Yes	MG	200	69.9	Qu et al. 2019
Sewage sludge and tea waste	No	MB	100	8.9	Fan et al. 2016

†, commercially available chars;

relatively low adsorption capacity and MB removal at higher MB concentration. Nonetheless, other examples can be found which showed similar adsorption capacity to that observed for PW-C.

When comparing the adsorption capacities, the displayed values for PW-C and some of the compared chars were roughly of the same magnitude order, as shown in Table 1. However, this was true only for non-activated chars (Lonappan et al. 2016; Sun et al. 2013; Chaukura et al. 2017; Fan et al. 2017; Hoslett et al. 2020), whereas activated chars showed adsorption capacity from one to two magnitudes of order greater than PW-C adsorption capacity at similar initial dye concentrations (Souza et al. 2006; Wu et al. 2022; Gupta et al. 2022; Li et al. 2021). Similarly, commercially available activated carbons displayed values one order of magnitude higher than PW-C values (Qu et al. 2019), supporting activation being a key step to obtain a high-sorbent char.

Despite the low adsorption capacity when compared to activated chars, it is important to recall here that the adsorbent used in this work is, in fact, a real waste. In other words, the reaction conditions used in the process were not chosen for its production. Therefore, it is interesting to observe that, still, it possesses suitable properties to perform wastewater remediation, which could be a basis for certifying this process as an end-of-waste application, and classify the char as a by-product, instead of a waste. Thus, future studies should

focus on conducting a life cycle assessment, to quantify the process environmental burdens, in accordance with European regulations (European Council 2008).

Moreover, the similarity of PW-C and biochars adsorption capacities showed that mixed plastic waste char could be used in place of biochar. This possibility could represent an important step toward achieving a sustainable society, for an important distinction between plastic-derived and biomass-derived chars; while biochars can be inserted into the soil to support several benefic changes to the soil characteristics (Tan et al. 2015; Chen et al. 2017), plastic-derived chars may not be suitable for such soil-remediation purposes. The European Delegated Regulation 2021/2088 (European Commission 2018) did not include non-biodegradable polymers among the pyrolysis products suitable for soil applications, thus showing that a plastic-derived char may not be suitable for such uses. Therefore, substituting biochars with plastic-derived chars could increase the amount of available biochars for agricultural use, improving soil conditions and possibly leading to enhanced agricultural crops yield.

Also, despite the relatively low adsorption capacity of PW-C, its nature as a residual waste makes such chars low-cost materials, as also stated in other literature works (Li et al. 2021; Essawy et al. 2017); therefore, the higher mass of PW-C needed to match higher-sorbent chars performances would not represent an economic issue. However, the higher PW-C mass needed might represent a technical limitation for

its use in a real process, leading to the necessity of conducting further studies on enhancing of its sorbent properties, through chemical or physical activation. Moreover, the heterogeneous nature of plastic wastes, despite being less heterogeneous than municipal ones (Zhang et al. 2020), could lead to plastic chars with different properties, potentially making activation an imperative step to obtain similarly performing materials over long time periods.

Nonetheless, PW-C as-it-is could represent a low-cost solution for low-concentration pollution wastewaters.

Adsorption mechanism, kinetics, and thermodynamics

Adsorption isotherms

Langmuir and Freundlich isotherms are represented in Fig. 4. Although both isotherms gave a good linear regression of equilibrium data, Langmuir isotherm showed a slightly higher quality fitting, with a 0.979 R^2 value, opposed to Freundlich isotherm 0.967 R^2 value. Langmuir isotherm was also reported as the most suitable model for MB adsorption onto various other substrates (Vadivelan and Kumar 2005; Fan et al. 2017), or the adsorption of other dyes onto plastic-derived adsorbent materials (Gupta et al. 2022; Li et al. 2021). This outcome suggested that PW-C was mainly characterized by a monolayer adsorption mechanism.

Langmuir and Freundlich isotherms parameters are reported in Table 2. When analyzing Langmuir separation factor R_L values, the values ranged from 0.25 at 20 mg/L to 0.063 at 100 mg/L initial MB concentration, suggesting the adsorption being a favored mechanism. Furthermore, R_L value decreasing with initial concentration increasing

suggested that higher initial MB concentration favored the adsorption.

Adsorption kinetics

Pseudo-first-order (PFO) model (Fig. 5A) returned an acceptable description of the adsorption ($0.79 < R^2 < 0.95$, depending on initial MB concentration and PW-C dosage), particularly during the first hour of the experiment. On the other hand, pseudo-second-order (PSO) model (Fig. 5B) gave a higher fitting of the overall adsorption data ($R^2 > 0.995$), demonstrating that MB adsorption on PW-C was better described by a pseudo-second-order process, in accordance with other literature works regarding adsorptions of dyes (Li et al. 2016, 2021). The adsorption process being accurately described by PSO model might suggest its nature as a chemisorption process (Ho and McKay 1999; Fan et al. 2017).

The PFO and PSO parameters are reported in Table 3. As shown, PSO kinetic constant decreased at increasing initial MB concentration. One possible reason of this trend might be the external boundary layer surrounding char particles becoming thicker (Chen and Bai 2013). Fan et al. proposed that at increasing concentration, intra-pore diffusion had higher influence on the rate-limiting step (Fan et al. 2017), similar to what was observed by Chen and Bai. They observed that at later stages of adsorption, the kinetic constant decreased, indicating that the already adsorbed molecules in the pores reduced the available free path for molecules in solution to diffuse into the pores (Chen and Bai 2013). The decrease in kinetic constant observed in this work reasonably matched the reported phenomena, as increasing the MB concentration would lead to less free path
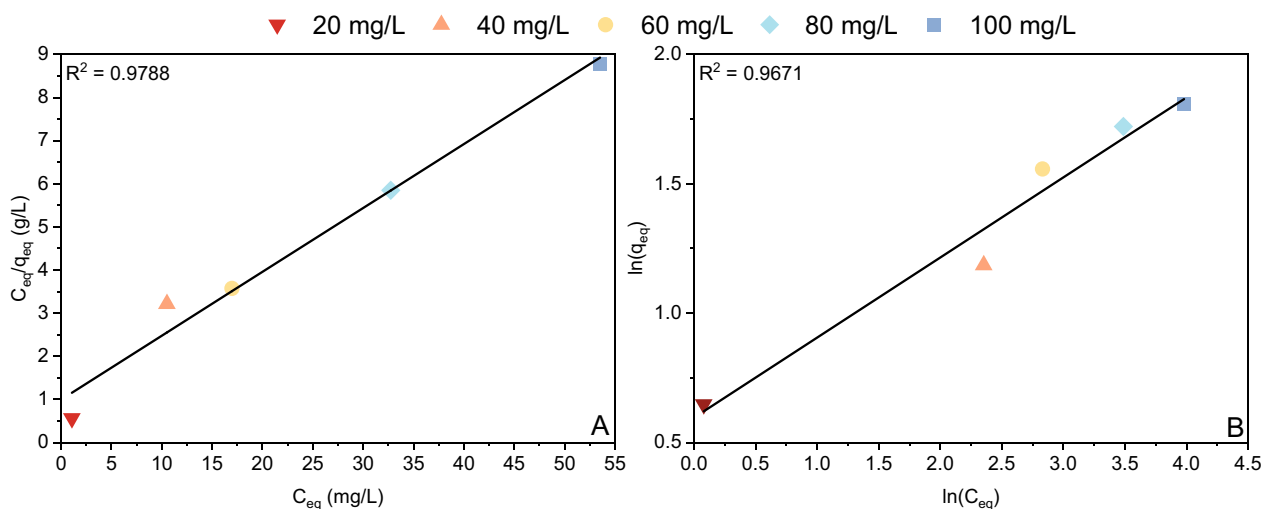

Fig. 4 Isotherm fittings of experimental data, at equilibrium. **A** Langmuir isotherm; **B** Freundlich isotherm. The data refer to operative conditions of 20 °C and a 2 g dose of PW-C

Table 2 Langmuir and Freundlich isotherms parameters for adsorption of MB on PW-C, at 2 g PW-C dosage and room temperature

Langmuir isotherm					
q_m (mg/g)	6.75 ± 0.58				
K_L (L/mg)	$0.15 \pm 4.90 \cdot 10^{-2}$				
R^2	0.979				
Initial MB concentration (mg/L)	20	40	60	80	100
R_L	0.25	0.14	0.10	0.08	0.06
Freundlich isotherm					
K_F	1.82 ± 0.17				
n	3.23 ± 0.35				
R^2	0.967				

space available in char pores. When increasing PW-C dosage, kinetic constant increased. This increase was likely tied both to available space in pores and boundary layer thickness, since higher quantity of char could have reduced the boundary layer thickness.

Once identified the kinetic model which describes in the most appropriate way the adsorption phenomena, the influence of external and internal diffusion phenomena was investigated employing intra-particle diffusion (IPD) and Boyd models. Both models convey similar information regarding the influence of diffusion phenomena; however, while Boyd model provided information regarding the rate-determining step over the entire adsorption course, intra-particle diffusion communicated further information on the prevalence of either diffusion phenomena over time, through a multi-linear fitting, displaying eventual changes in the occurring transport phenomena in different phases of the adsorption process.

Figure 6 shows Boyd model data fitting for some selected initial conditions (20 and 80 mg/L initial MB, with 2 g PW-C dosage). As shown in Table 3, the intercept of the Boyd model lines decreased at increasing MB concentration or decreasing PW-C dosage. This was possibly explained by the driving force increasing more than the boundary layer thickness, therefore resulting in MB molecules more easily overcoming the resistance to external mass transfer. Regarding the intra-particle diffusion model (Fig. 6C, D), multi-linear fitting suggested that the nature of the rate-determining mass transfer phenomena shifted with time, external mass transfer being the rate-determining step in the first hour of adsorption and mass transfer into the pores being more influential in the second phase of adsorption, in accordance with other literature works findings (Chen and Bai 2013; Fu et al. 2015). The increasing C coefficient values (Table 3) showed that, with MB initial concentration increasing or PW-C dosage decreasing, the

external mass transfer had greater influence on the first hour of adsorption.

Notably, the combined use of Boyd and IPD models showed a shift in mass-transfer phenomena. Since Boyd model intercepts was greater than zero, we can suppose that the adsorption process kinetics was mainly determined by external mass transfer. However, the decreasing intercepts showed a progressive reduction in external transfer phenomena influence on the overall kinetics. Simultaneously, IPD model showed an increasing k_{p1} (tied to external mass transfer) and decreasing k_{p2} (tied to intra-pore diffusion), demonstrating an increasingly slowing of the internal mass transfer and thus an increase in its role in determining the overall process kinetics. The effect of intra-pore diffusion was therefore shown to possibly be relevant, especially at increasing MB concentration, even if not being the principal rate-determining step. Similar behavior was observed at decreasing PW-C dosage (Vadivelan and Kumar 2005).

The similar behavior of PW-C kinetics and adsorption isotherms suggested and reinforced the possibility of substituting non-activated biomass-derived chars with non-activated plastic-derived chars, as discussed in the adsorption performance results section, showing the possibility of integrating the latters in the industry as an indirect support to biochars use in agriculture.

Adsorption thermodynamics

To further analyze the thermodynamic aspects of the adsorption, Van't Hoff equations were utilized to determine adsorption enthalpy, entropy, and Gibbs free energy.

Langmuir K_L constant values increased at increasing adsorption temperature, suggesting an increment of adsorbed MB mass, due to increasing value of equilibrium constant K. Linear regression of $\ln(K)$ vs $1/T$ plot gave adsorption enthalpy and entropy values, reported in Table 4. Enthalpy and entropy of adsorption were assumed constant based on Langmuir isotherm good fitting of the data. Gibbs free energy was calculated at each temperature (Table 4).

The investigation revealed Gibbs free energy to become more negative at increasing adsorption temperature, thus indicating a more spontaneous adsorption at higher temperatures. Compared to other literature works (Hassan et al. 2014; Fu et al. 2015; Fan et al. 2017), MB adsorption on PW-C was shown to be a spontaneous process. The adsorption enthalpy was equal to 7.18 kJ/mol. As reported in other literature works, a ΔH^0 between 0 and 25 kJ/mol is characteristic of physisorption mechanisms (Fan et al. 2017; Fu et al. 2015), whereas values between 40 and 200 kJ/mol are typical of chemisorption mechanisms (Fan et al. 2017). Thus, positive, albeit close to zero, enthalpy determined the adsorption to be prevalently characterized by a physisorption mechanism. The entropy value was in line with
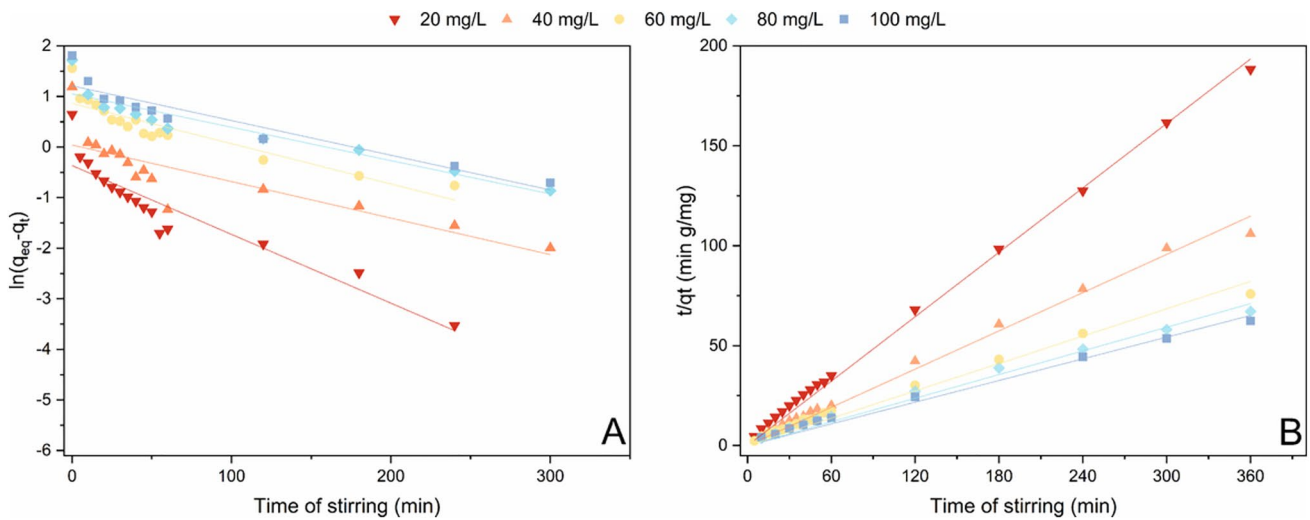
Fig. 5 Linear regression of pseudo-first-order and pseudo-second-order kinetic models of MB adsorption onto PW-C, at various initial MB concentration and 2 g PW-C dosage. **A** pseudo-first-order model; **B** pseudo-second-order model. All data were collected at 20 °C

Table 3 Studied kinetic model parameters for MB adsorption on PW-C, at different char doses, and initial MB concentrations. All data were collected at 20 °C. The "C" and "R^2" parameters of intra-parti- cle diffusion model were referred exclusively to the first linear segment of the fitted data

Initial MB concentration (mg/L)	PW-C dosage (g)	Pseudo-first order model		Pseudo-second order model		
		k_I (1/min)	R^2	k_II (g/(mg min))	q_eq (mg/g)	R^2
20	2.0	$1.36 \cdot 10^{-2} \pm 1.45 \cdot 10^{-3}$	0.863	$6.56 \cdot 10^{-2} \pm 5.70 \cdot 10^{-3}$	$1.93 \pm 1.00 \cdot 10^{-2}$	0.999
40		$1.15 \cdot 10^{-2} \pm 1.51 \cdot 10^{-3}$	0.805	$2.67 \cdot 10^{-2} \pm 5.40 \cdot 10^{-3}$	$3.38 \pm 3.90 \cdot 10^{-2}$	0.998
60		$0.80 \cdot 10^{-2} \pm 9.60 \cdot 10^{-4}$	0.830	$1.19 \cdot 10^{-2} \pm 1.20 \cdot 10^{-3}$	$4.78 \pm 8.90 \cdot 10^{-2}$	0.995
80		$0.77 \cdot 10^{-2} \pm 5.00 \cdot 10^{-4}$	0.941	$0.76 \cdot 10^{-2} \pm 1.15 \cdot 10^{-4}$	$5.68 \pm 9.90 \cdot 10^{-2}$	0.997
100		$0.77 \cdot 10^{-2} \pm 4.90 \cdot 10^{-4}$	0.950	$0.66 \cdot 10^{-2} \pm 7.60 \cdot 10^{-4}$	$6.22 \pm 3.70 \cdot 10^{-2}$	0.998
20	0.5	$0.09 \cdot 10^{-2} \pm 6.70 \cdot 10^{-4}$	0.923	$1.07 \cdot 10^{-2} \pm 7.00 \cdot 10^{-4}$	$4.99 \pm 5.60 \cdot 10^{-2}$	0.998
	1.0	$0.69 \cdot 10^{-2} \pm 7.90 \cdot 10^{-4}$	0.872	$2.13 \cdot 10^{-2} \pm 5.00 \cdot 10^{-3}$	$3.44 \pm 4.90 \cdot 10^{-2}$	0.998
	1.5	$1.90 \cdot 10^{-2} \pm 1.73 \cdot 10^{-3}$	0.903	$5.83 \cdot 10^{-2} \pm 5.80 \cdot 10^{-3}$	$2.32 \pm 1.70 \cdot 10^{-2}$	0.999
	2.0	$1.36 \cdot 10^{-2} \pm 1.45 \cdot 10^{-3}$	0.863	$6.56 \cdot 10^{-2} \pm 5.70 \cdot 10^{-3}$	$1.93 \pm 1.00 \cdot 10^{-2}$	0.999
	2.5	$1.14 \cdot 10^{-2} \pm 1.54 \cdot 10^{-3}$	0.786	$1.34 \cdot 10^{-1} \pm 1.70 \cdot 10^{-2}$	$1.55 \pm 6.9 \cdot 10^{-3}$	0.999

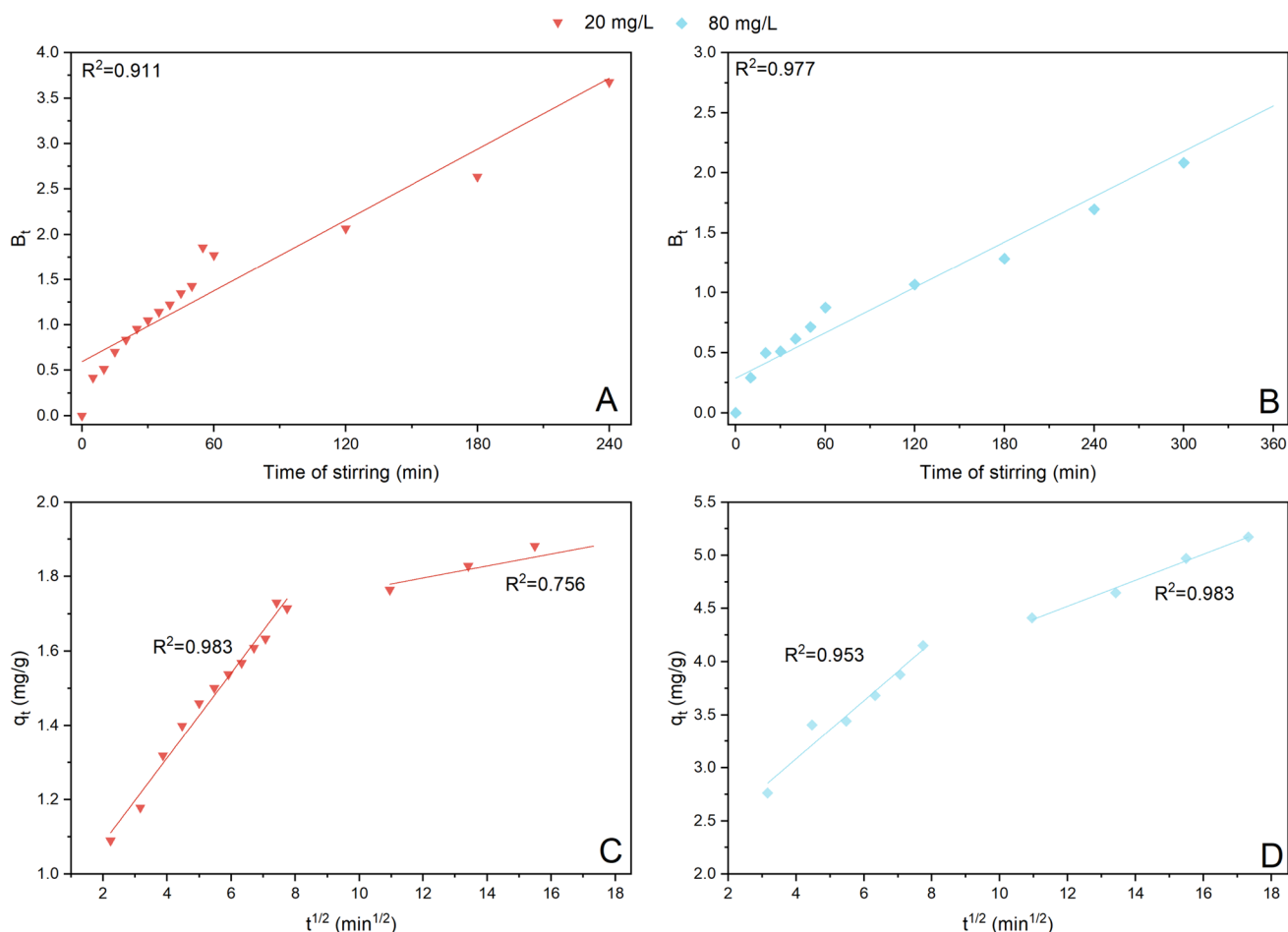| Initial MB concentration (mg/L)	PW-C dosage (g)	Boyd model		Intra-particle diffusion model			
		Intercept	R^2	k_p (mg/(g min$^{1/2}$))		C (mg/g)	R^2
				1st segment, k_p1	2nd segment, k_p2		
20	2.0	$0.60 \pm 9.50 \cdot 10^{-2}$	0.911	$0.11 \pm 4.70 \cdot 10^{-3}$	$1.60 \cdot 10^{-2} \pm 6.40 \cdot 10^{-3}$	$0.85 \pm 2.70 \cdot 10^{-2}$	0.983
40		$0.66 \pm 8.80 \cdot 10^{-2}$	0.881	$0.16 \pm 1.70 \cdot 10^{-2}$	$4.10 \cdot 10^{-2} \pm 2.60 \cdot 10^{-3}$	$1.60 \pm 9.90 \cdot 10^{-2}$	0.919
60		$0.32 \pm 5.10 \cdot 10^{-2}$	0.914	$0.27 \pm 2.30 \cdot 10^{-2}$	$9.50 \cdot 10^{-2} \pm 1.30 \cdot 10^{-2}$	1.48 ± 0.13	0.934
80		$0.30 \pm 5.70 \cdot 10^{-2}$	0.977	$0.27 \pm 3.00 \cdot 10^{-2}$	$1.08 \cdot 10^{-1} \pm 6.30 \cdot 10^{-3}$	1.99 ± 0.18	0.953
100		$0.24 \pm 5.20 \cdot 10^{-2}$	0.983	$0.37 \pm 5.80 \cdot 10^{-2}$	$1.05 \cdot 10^{-1} \pm 1.80 \cdot 10^{-3}$	1.49 ± 0.34	0.912
20	0.5	$0.23 \pm 4.80 \cdot 10^{-2}$	0.960	$0.34 \pm 8.80 \cdot 10^{-3}$	$0.14 \pm 2.30 \cdot 10^{-2}$	$1.09 \pm 5.00 \cdot 10^{-2}$	0.993
	1.0	0.59 ± 0.12	0.917	$0.09 \pm 2.10 \cdot 10^{-2}$	$0.05 \pm 2.00 \cdot 10^{-3}$	2.21 ± 0.12	0.818
	1.5	$0.53 \pm 7.10 \cdot 10^{-2}$	0.954	$0.10 \pm 4.70 \cdot 10^{-3}$	$1.60 \cdot 10^{-2} \pm 8.80 \cdot 10^{-3}$	$1.30 \pm 2.70 \cdot 10^{-2}$	0.977
	2.0	$0.59 \pm 9.50 \cdot 10^{-2}$	0.911	$0.11 \pm 4.70 \cdot 10^{-3}$	$1.60 \cdot 10^{-2} \pm 6.40 \cdot 10^{-3}$	$0.85 \pm 2.70 \cdot 10^{-2}$	0.983
	2.5	1.03 ± 0.14	0.831	$0.07 \pm 4.30 \cdot 10^{-3}$	$1.30 \cdot 10^{-2} \pm 1.30 \cdot 10^{-3}$	$0.92 \pm 2.40 \cdot 10^{-2}$	0.965

Fig. 6 Adsorption data fitting of Boyd and intra-particle diffusion kinetic models. For simplicity, only one line per graph was reported. **a** Boyd model, 2 g PW-C dosage, 20 mg/L initial MB concentration; **b** Boyd model, 2 g PW-C dosage, 80 mg/L initial MB concentration; **c** intra-particle diffusion model, 2 g PW-C dosage, 20 mg/L initial MB concentration; **d** intra-particle diffusion model, 2 g PW-C dosage, 80 mg/L initial MB concentration. All data were collected at 20 °C

other literature findings (Fu et al. 2015; Fan et al. 2017), indicating that MB adsorption increased randomness at solid/liquid interface (Ninh et al. 2023; Fan et al. 2017), as consequence of PW-C surface structure being modified during MB adsorption (Fu et al. 2015), and of MB molecules overcoming the adsorption activation energy barrier (Hassan et al. 2014).

Thermodynamic parameter analysis revealed that adsorption occurred mainly by a physisorption process, despite PSO kinetics suggesting chemisorption to be the prevalent phenomena. To the authors' knowledge, other instances of PSO-abiding physisorption were observed in the literature (Fu et al. 2015; Chen and Bai 2013), revealing the co-occurrence of both physi- and chemisorption (Wu et al. 2022; Fan et al. 2017). The adsorption process may hence be a rather complex phenomenon, likely involving some occurrences of chemisorption, other than prevalently occurring as physisorption.

Table 4 Thermodynamic parameters of MB adsorption onto plastic waste-derived char

T (°C)	K	ΔG^0 (kJ/mol)	ΔH^0 (kJ/mol)	ΔS^0 (kJ/(mol·K))
20	47,657	− 26.2	7.18 ± 0.80	$0.11 \pm 2.59 \cdot 10^{-3}$
35	53,310	− 27.9		
45	61,228	− 29.1		
55	64,377	− 30.2		

Adsorption mechanism

To propose a MB adsorption mechanism, several aspects of the conducted data analysis and investigations were considered. As discussed in Section "Adsorption kinetics" and "Adsorption thermodynamics," the adsorption process likely occurred as a predominantly physisorption process, characterized, to a lesser extent, by occurrences of chemisorption

phenomena, as suggested by thermodynamics and pseudo-second-order kinetics, respectively. Both physisorption and chemisorption phenomena were compatible with Langmuir isotherm assumption of adsorption occurring as a monolayer phenomenon.

Regarding the physisorption phenomena, FT-IR analysis of post-adsorption PW-C (Fig. 2D) gave valuable information. The band observed between roughly 1050 and 850 cm^{-1} could represent the formation of hydrogen bonds involving the MB nitrogen atoms and OH groups, as also found by Fan et al. 2017, or possibly other hydrogen atoms contained in PW-C surface functional groups. Similar hydrogen bonds may also have established, albeit to a lesser extent, between MB sulfur atom and hydrogen atoms on PW-C surface (Ovchinnikov et al. 2016). Hydrogen bonds caused an overlapping of signals with the region near 870–850 cm^{-1}, which identifies phenol groups (Li et al. 2021), thus not allowing to obtain unambiguous information. Phenol groups, alongside other aromatic compounds on PW-C surface, may have participated in formation of π–π interactions with the MB aromatic ring. The interaction between aromatic rings was supported by FT-IR analysis (Fig. 2D), which showed a shift of the band located in the 1500–1250 cm^{-1} region and the peak located at roughly 640 cm^{-1} (Ovchinnikov et al. 2016; Li et al. 2021; Fu et al. 2015).

Lastly, Si–O–Si groups belonging to SiO$_2$ might have been involved in the physisorption phenomena, eventually being responsible for n–π interactions between the oxygen lone electron pairs and the delocalized electrons in orbital π of MB aromatic ring (Khraisheh et al. 2005; Fan et al. 2017). The proposed mechanism is illustrated and summarized in Fig. 7.

waste management processes. The kinetic was investigated to provide data for the design of a suitable treatment process, and it was observed to be well described by pseudo-second-order kinetics model ($R^2 > 0.99$), while Langmuir isotherm returned a good fit of experimental data ($R^2 = 0.98$), revealing MB to prevalently form a monolayer during the adsorption. External mass transfer was observed to be the rate-determining step, coupled with a non-negligible influence of intra-pore diffusion after the first hour of adsorption. The adsorption was observed to be a spontaneous ($\Delta G^0 \approx -26/-30$ kJ/mol) and endothermic ($\Delta H^0 = 7.18$ kJ/mol) process, with the latter suggesting a predominant physisorption phenomenon.

In conclusion, the investigated char represents a suitable material to treat low-pollutant-concentration wastewaters. The innovative utilization of a char derived from plastic waste pyrolysis highlights two important benefits for the society, i.e., the exploitation of a waste as cost-effective sorbent in the sustainable wastewater treatment, possibly representing an end-of-waste application. Other issues remain to be solved, such as the scalability, application with real multi-component wastewater streams, and the regeneration. The latter is a key issue because it is related to the economic efficiency of the entire process. Different techniques can be used, commonly differentiated in decomposition or desorption methods. Activation emerged as another relevant aspect, contributing to elevate the char sorbent properties to compete with commercial activated carbons' adsorption performances. However, being the present work a preliminary investigation on the suitability of plastic-derived char as adsorbent, these aspects were not taken into account and will be explored in further studies.
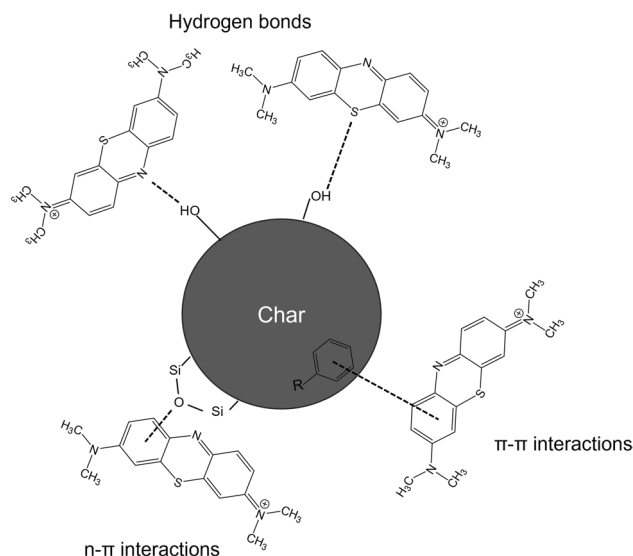
Conclusion

In this work, the utilization of a char derived from a plastic waste pyrolysis plant (pilot scale) was studied for the first time as adsorbent for methylene blue polluted wastewater.

The multiple characterization allowed to observe the prevalence of inorganic rod-like structures, in which Si was a key element, while the organic compounds were mainly identified as aromatic in nature, providing interactions via π–π bonds.

The adsorption tests revealed that using 2 g of char for treating low-concentration methylene blue wastewaters (200 mL, 20 mg/L initial MB concentration) achieved up to 96% of pollutant removal. Interestingly, the adsorption capacity reached 5.8 mg/g, which is within the range of other systems present in literature. This is an important result since the used char was an actual waste obtained from a waste-to-energy process, and hence represents a low-cost sorbent material derived from plastic

Fig. 7 Summary of the proposed mechanisms for MB adsorption on PW-C

Overall, this study not only contributes to the field of environmental remediation but makes a significant stride toward eco-friendly materials in the realm of plastic waste management.

Data availability The datasets used and/or analyzed during the current study are available from the corresponding author on request.

Declarations

Conflict of interests The authors have no relevant financial or non-financial interests to disclose.

Ethics approval and consent to participate Since this study did not recruit any human and/or animal subjects, this section does not apply.

Consent for publication The authors confirm that the final version of the manuscript has been reviewed, approved, and consented for publications by all authors.

References

Achari VS, Lopez RM, Rajalakshmi AS, Jayasree S, Shibin OM, John D, Sekkar V (2021) Microporous carbon with highly dispersed nano-lanthanum oxide (La_2O_3) for enhanced adsorption of methylene blue. Sep Purif Technol 279:119626. https://doi.org/10.1016/j.seppur.2021.119626

Ahmed MJ, Hameed BH (2020) Insight into the co-pyrolysis of different blended feedstocks to biochar for the adsorption of organic and inorganic pollutants : a review. J Clean Prod 265:121762. https://doi.org/10.1016/j.jclepro.2020.121762

Ahmetli G, Kocaman S, Ozaytekin I, Bozkurt P (2013) Epoxy composites based on inexpensive char filler obtained from plastic waste and natural resources. Polym Compos 34(4):500–509. https://doi.org/10.1002/pc.22452

Antelava A, Jablonska N, Constantinou A, Manos G, Salaudeen SA, Dutta A, Al-Salem SM (2021) Energy potential of plastic waste valorization: a short comparative assessment of pyrolysis versus gasification. Energy Fuels 35(5):3558–3571. https://doi.org/10.1021/acs.energyfuels.0c04017

Baloo L, Isa MH, Sapari NB, Jagaba AH, Wei LJ, Yavari S, Razali R, Vasu R (2021) Adsorptive removal of methylene blue and acid orange 10 dyes from aqueous solutions using oil palm wastes-derived activated carbons. Alex Eng J 60(6):5611–5629. https://doi.org/10.1016/j.aej.2021.04.044

Boyd GE, Adamson AW, Myers LS Jr (1947) The exchange adsorption of ions from aqueous solutions by organic zeolites; kinetics. J Am Chem Soc 69(11):2571–2920. https://doi.org/10.1021/ja01203a066

Chaukura N, Murimba EC, Gwenzi W (2017) Synthesis, characterisation and methyl orange adsorption capacity of ferric oxide–biochar nano-composites derived from pulp and paper sludge. Appl Water Sci 7(5):2175–2186. https://doi.org/10.1007/s13201-016-0392-5

Chen L, Bai Bo (2013) Equilibrium, kinetic, thermodynamic, and in situ regeneration studies about methylene blue adsorption by the raspberry-like TiO_2@ yeast microspheres. Ind Eng Chem Res 52:15568–15577. https://doi.org/10.1021/ie4020364

Chen Y, Zhang X, Chen W, Yang H, Chen H (2017) The structure evolution of biochar from biomass pyrolysis and its correlation with gas pollutant adsorption performance. Bioresour Technol. https://doi.org/10.1016/j.biortech.2017.08.138

Chen Xi, Wang Y, Zhang L (2021) Recent progress in the chemical upcycling of plastic wastes. Chemsuschem 14(19):4137–4151. https://doi.org/10.1002/cssc.202100868

Cossu R, Fiore S, Lai T, Luciano A, Mancini G, Ruffino B, Viotti P, Zanetti MC (2014) Review of Italian experience on automotive shredder residue characterization and management. Waste Manag 34(10):1752–1762. https://doi.org/10.1016/j.wasman.2013.11.014

Dahlbo H, Poliakova V, Mylläri V, Sahimaa O, Anderson R (2018) Recycling potential of post-consumer plastic packaging waste in Finland. Waste Manage 71:52–61. https://doi.org/10.1016/j.wasman.2017.10.033

Dai Y, Zhang N, Xing C, Cui Q, Sun Q (2019) The adsorption, regeneration and engineering applications of biochar for removal organic pollutants: a review. Chemosphere. https://doi.org/10.1016/j.chemosphere.2019.01.161

Dao MU, Le HS, Hoang HY, Tran VA, Doan VD, Le TT, Sirotkin A, Le VT (2021) Natural core-shell structure activated carbon beads derived from *Litsea Glutinosa* seeds for removal of methylene blue: facile preparation, characterization, and adsorption properties. Environ Res 198:110481. https://doi.org/10.1016/j.envres.2020.110481

de Souza MJ, da Costa Júnior NB, Almeida LE, da Silva Vieira EF, Cestari AR, de Fátima GI, Carreño NLV, Barreto LS (2006) Kinetic and calorimetric study of the adsorption of dyes on

mesoporous activated carbon prepared from coconut coir dust. J Colloid Interface Sci 298(2):515–522. https://doi.org/10.1016/j.jcis.2006.01.021

Dogu O, Pelucchi M, Van de Vijver R, Van Steenberge PH, D'hooge DR, Cuoci A, Mehl M, Frassoldati A, Faravelli T, Van Geem KM (2021) The chemistry of chemical recycling of solid plastic waste via pyrolysis and gasification: state-of-the-art, challenges, and future directions. Prog Energy Combust Sci. https://doi.org/10.1016/j.pecs.2020.100901

El-Shafey EI, Ali SNF, Al-Busafi S, Al-Lawati HAJ (2016) Preparation and characterization of surface functionalized activated carbons from date palm leaflets and application for methylene blue removal. J Environ Chem Eng 4(3):2713–2724. https://doi.org/10.1016/j.jece.2016.05.015

Eriksen MK, Pivnenko K, Faraca G, Boldrin A, Astrup TF (2020) Dynamic material flow analysis of PET, PE, and PP flows in Europe: evaluation of the potential for circular economy. Environ Sci Technol 54(24):16166–16175. https://doi.org/10.1021/acs.est.0c03435

Essawy NA, El SM, Ali HA, Farag AH, Konsowa ME, Hamad HA (2017) Green synthesis of graphene from recycled PET bottle wastes for use in the adsorption of dyes in aqueous solution. Ecotoxicol Environ Saf 145:57–68. https://doi.org/10.1016/j.ecoenv.2017.07.014

European Commission (2008) Directive 2008/98/EC of the European Parliament and of the Council of 19 November 2008 on waste and repealing certain directives. Official Journal of European Union. http://eur-lex.europa.eu/LexUriServ/LexUriServ.do?uri=OJ:L:2008:312:0003:01:ES:HTML

European Commission (2018) Commission delegated regulation (EU) 2021/2086 of 5 July 2021 amending annexes II and IV to regulation (EU) 2019/1009, 2016. https://eur-lex.europa.eu/legal-content/EN/ALL/?uri=CELEX:32021R2088

European Council (2008). Directive 2008/98/EC of the European Parliament and of the Council of 19 November 2008 on waste and repealing certain directives

Europe Plastic (2022) Plastics—the facts 2022 https://plasticseurope.org/knowledge-hub/plastics-the-facts-2022/

Fan S, Tang J, Wang Yi, Li H, Zhang H, Tang J, Wang Z, Li X (2016) Biochar prepared from co-pyrolysis of municipal sewage sludge and tea waste for the adsorption of methylene blue from aqueous solutions: kinetics, isotherm, thermodynamic and mechanism. J Mol Liq 220:432–441. https://doi.org/10.1016/j.molliq.2016.04.107

Fan S, Wang Yi, Wang Z, Tang J, Tang J, Li X (2017) Removal of methylene blue from aqueous solution by sewage sludge-derived biochar: adsorption kinetics, equilibrium, thermodynamics and mechanism. J Environ Chem Eng 5(1):601–611. https://doi.org/10.1016/j.jece.2016.12.019

Ferrari A, Robertson J (2000) Interpretation of Raman spectra of disordered and amorphous carbon. Phys Rev B Condens Matter Mater Phys 61(20):14095–14107. https://doi.org/10.1103/PhysRevB.61.14095

Fu J, Chen Z, Wang M, Liu S, Zhang J, Zhang J, Han R, Qun Xu (2015) Adsorption of methylene blue by a high-efficiency adsorbent (polydopamine microspheres): kinetics, isotherm, thermodynamics and mechanism analysis. Chem Eng J 259:53–61. https://doi.org/10.1016/j.cej.2014.07.101

Fuente-Cuesta A, Diamantopoulou I, Lopez-Anton MA, Martínez-Tarazona MR, Sakellaropoulos GP (2015) Study of mercury adsorption by low-cost sorbents using kinetic modeling. Ind Eng Chem Res 54(21):5572–5579. https://doi.org/10.1021/acs.iecr.5b00262

Godinho D, Dias D, Bernardo M, Lapa N, Fonseca I, Lopes H, Pinto F (2017) Adding value to gasification and co-pyrolysis chars as

removal agents of Cr^{3+}. J Hazard Mater 321:173–182. https://doi.org/10.1016/j.jhazmat.2016.09.006

Gupta V, Bhardwaj NK, Rawal RK (2022) Removal of colour and lignin from paper mill wastewater using activated carbon from plastic mix waste. Int J Environ Sci Technol 19(4):2641–2658. https://doi.org/10.1007/s13762-021-03263-9

Harussani MM, Rashid U, Sapuan SM, Abdan K (2021) Low-temperature thermal degradation of disinfected Covid-19 non-woven polypropylene—based isolation gown wastes into carbonaceous char. Polymers. https://doi.org/10.3390/polym13223980

Hassan AF, Abdel-Mohsen AM, Fouda MMG (2014) Comparative study of calcium alginate, activated carbon, and their composite beads on methylene blue adsorption. Carbohydr Polym 102(1):192–198. https://doi.org/10.1016/j.carbpol.2013.10.104

Ho YS, McKay G (1999) Pseudo-second order model for sorption processes. Process Biochem 34(5):451–465. https://doi.org/10.1016/S0032-9592(98)00112-5

Hoslett J, Ghazal H, Ahmad D, Jouhara H (2019) Removal of copper ions from aqueous solution using low temperature biochar derived from the pyrolysis of municipal solid waste. Sci Total Environ 673:777–789. https://doi.org/10.1016/j.scitotenv.2019.04.085

Hoslett J, Ghazal H, Mohamad N, Jouhara H (2020) Removal of methylene blue from aqueous solutions by biochar prepared from the pyrolysis of mixed municipal discarded material. Sci Total Environ 714:136832. https://doi.org/10.1016/j.scitotenv.2020.136832

Joshiba GJ, Kumar PS, Rangasamy G, Ngueagni PT, Pooja G, Balji GB, El-Serehy HA (2022) Iron doped activated carbon for effective removal of tartrazine and methylene blue dye from the aquatic systems: kinetics, isotherms, thermodynamics and desorption studies. Environ Res 215:114317. https://doi.org/10.1016/j.envres.2022.114317

Khraisheh MAM, Al-Ghouti MA, Allen SJ, Ahmad MN (2005) Effect of OH and silanol groups in the removal of dyes from aqueous solution using diatomite. Water Res 39(5):922–932. https://doi.org/10.1016/j.watres.2004.12.008

Ko, Kwang Hyun, Tae Jun Park, Veena Sahajwalla, and Aditya Rawal. 2021. "Complex Microstructural Evolution in High Temperature Pyrolysis of Plastic and Biomass." *Fuel* 291 (April 2020): 120153. https://doi.org/10.1016/j.fuel.2021.120153.

Lai C, He H, Xie W, Fan S, Huang H, Wang Y, Huang B, Pan X (2022) Adsorption and photochemical capacity on 17α-ethinylestradiol by char produced in the thermo treatment process of plastic waste. J Hazard Mater 423:127066. https://doi.org/10.1016/j.jhazmat.2021.127066

Li D, Yan J, Liu Z, Liu Z (2016) Adsorption kinetic studies for removal of methylene blue using activated carbon prepared from sugar beet pulp. Int J Environ Sci Technol 13(7):1815–1822. https://doi.org/10.1007/s13762-016-1012-5

Li Z, Chen K, Chen Z, Li W, Biney BW, Guo A, Liu D (2021) Removal of malachite green dye from aqueous solution by adsorbents derived from polyurethane plastic waste. J Environ Chem Eng 9(1):104704. https://doi.org/10.1016/j.jece.2020.104704

Lonappan L, Rouissi T, Das RK, Brar SK, Ramirez AA, Verma M, Surampalli RY, Valero JR (2016) Adsorption of methylene blue on biochar microparticles derived from different waste materials. Waste Manag 49:537–544. https://doi.org/10.1016/j.wasman.2016.01.015

Lopez G, Artetxe M, Amutio M, Alvarez J, Bilbao J, Olazar M (2018) Recent advances in the gasification of waste plastics. A critical overview. Renew Sustain Energy Rev 82:576–596. https://doi.org/10.1016/j.rser.2017.09.032

Martín-Lara MA, Piñar A, Ligero A, Blázquez G, Calero M (2021) Characterization and use of char produced from pyrolysis of post-consumer mixed plastic waste. Water (switzerland) 13(9):1188. https://doi.org/10.3390/w13091188

Miandad R, Rajeev Kumar MA, Barakat CB, Aburiazaiza AS, Nizami AS, Rehan M (2018) Untapped conversion of plastic waste char into carbon-metal LDOs for the adsorption of congo red. J Colloid Interface Sci 511:402–410. https://doi.org/10.1016/j.jcis.2017.10.029

Mun H, Ri C, Liu Q, Tang J (2022) Characteristics of ball-milled PET plastic char for the adsorption of different types of aromatic organic pollutants. Environ Sci Pollut Res 29(51):77685–77697. https://doi.org/10.1007/s11356-022-21143-8

Nanda S, Berruti F (2021) Thermochemical conversion of plastic waste to fuels: a review. Environ Chem Lett 19(1):123–148. https://doi.org/10.1007/s10311-020-01094-7

Ngueagni PT, Kumar PS, Woumfo ED, Abilarasu A, Joshiba GJ, Carolin CF, Prasannamedha G, Fotsing PN, Siewe M (2021) Effectiveness of a biogenic composite derived from cattle horn core/iron nanoparticles via wet chemical impregnation for cadmium (II) removal in aqueous solution. Chemosphere 272:129806. https://doi.org/10.1016/j.chemosphere.2021.129806

Ninh PTT, Tuyen TN, Dat ND, Nguyen ML, Dong NT, Chao HP, Tran HN (2023) Two-stage preparation of highly mesoporous carbon for super-adsorption of paracetamol and tetracycline in water: important contribution of pore filling and π–π interaction. Environ Res 218:114927. https://doi.org/10.1016/j.envres.2022.114927

Obeso JL, López-Olvera A, Flores CV, Martínez-Ahumada E, Paz R, Viltres H, Islas-Jácome A et al (2022) Methylene blue adsorption in DUT-5: relatively strong host–guest Interactions elucidated by FTIR, solid-state NMR, and XPS. J Mol Liq 368:120758. https://doi.org/10.1016/j.molliq.2022.120758

Ovchinnikov OV, Evtukhova AV, Kondratenko TS, Smirnov MS, Khokhlov VY, Erina OV (2016) Manifestation of intermolecular interactions in FTIR spectra of methylene blue molecules. Vib Spectrosc 86:181–189. https://doi.org/10.1016/j.vibspec.2016.06.016

Perdikatsis B, Burzlaff H (1981) Strukturverfeinerung am talk Mg$_3$[(OH)$_2$Si$_4$O$_{10}$]. Z Fur Kristallographie—New Cryst Struct 156(3–4):177–186. https://doi.org/10.1524/zkri.1981.156.3-4.177

Qu W, Yuan T, Yin G, Shiai Xu, Zhang Q, Hongjun Su (2019) Effect of properties of activated carbon on malachite green adsorption. Fuel 249:45–53. https://doi.org/10.1016/j.fuel.2019.03.058

Roosen M, Mys N, Kusenberg M, Billen P, Dumoulin A, Dewulf Jo, Van Geem KM, Ragaert K, De Meester S (2020) Detailed analysis of the composition of selected plastic packaging waste products and its implications for mechanical and thermochemical recycling. Environ Sci Technol 54(20):13282–13293. https://doi.org/10.1021/acs.est.0c03371

Sahoo TR, Prelot B (2020) Adsorption processes for the removal of contaminants from wastewater: the perspective role of nanomaterials and nanotechnology. In: Nanomaterials for the detection and removal of wastewater pollutants. Elsevier, 161–222. https://doi.org/10.1016/B978-0-12-818489-9.00007-4

Santoso E, Ediati R, Kusumawati Y, Bahruji H, Sulistiono DO, Prasetyoko D (2020) Review on recent advances of carbon based adsorbent for methylene blue removal from waste water. Mater Today Chem. https://doi.org/10.1016/j.mtchem.2019.100233

Sergiienko R, Shibata E, Kim S, Kinota T, Nakamura T (2009) Nanographite structures formed during annealing of disordered carbon containing finely-dispersed carbon nanocapsules with iron carbide cores. Carbon 47(4):1056–1065. https://doi.org/10.1016/j.carbon.2008.12.029

Sharuddin SDA, Abnisa F, Daud WMAW, Aroua MK (2016) A review on pyrolysis of plastic wastes. Energy Convers Manag. https://doi.org/10.1016/j.enconman.2016.02.037

Singh E, Kumar A, Khapre A, Saikia P, Shukla SK, Kumar S (2020) Efficient removal of arsenic using plastic waste char : prevailing mechanism and sorption performance. J Water Process Eng 33:101095. https://doi.org/10.1016/j.jwpe.2019.101095

Singh E, Kumar A, Mishra R, You S, Singh L, Kumar S, Kumar R (2021) Pyrolysis of waste biomass and plastics for production of biochar and its use for removal of heavy metals from aqueous solution. Bioresour Technol 320:124278. https://doi.org/10.1016/j.biortech.2020.124278

Sun L, Wan S, Luo W (2013) Biochars prepared from anaerobic digestion residue, palm bark, and Eucalyptus for adsorption of cationic methylene blue dye: characterization, equilibrium, and kinetic studies. Bioresour Technol 140:406–413. https://doi.org/10.1016/j.biortech.2013.04.116

Tan X, Liu Y, Zeng G, Wang X, Hu X, Gu Y, Yang Z (2015) Application of biochar for the removal of pollutants from aqueous solutions. Chemosphere. https://doi.org/10.1016/j.chemosphere.2014.12.058

Tomul F, Arslan Y, Kabak B, Trak D, Kendüzler E, Lima EC, Tran HN (2020) Peanut shells-derived biochars prepared from different carbonization processes: comparison of characterization and mechanism of naproxen adsorption in water. Sci Total Environ. https://doi.org/10.1016/j.scitotenv.2020.137828

Tran TH, Le AH, Pham TH, La DD, Nguyen XC, Nadda AK, Chang SW, Chung WJ, Nguyen DD, Nguyen DT (2022) A sustainable, low-cost carbonaceous hydrochar adsorbent for methylene blue adsorption derived from corncobs. Environ Res 212:113178. https://doi.org/10.1016/j.envres.2022.113178

Travália BM, Forte MBS (2020a) New proposal in a biorefinery context: recovery of acetic and formic acids by adsorption on hydrotalcites. J Chem Eng Data 65:4503–4511. https://doi.org/10.1021/acs.jced.0c00340

Travália BM, Forte MBS (2020b) New proposal in a biorefinery context: recovery of acetic and formic acids by adsorption on hydrotalcites. J Chem Eng Data 65(9):4503–4511. https://doi.org/10.1021/acs.jced.0c00340

United Nations (2015) Transforming our world: the 2030 agenda for sustainable development

Vadivelan V, Kumar KV (2005) Equilibrium, kinetics, mechanism, and process design for the sorption of methylene blue onto rice husk. J Colloid Interface Sci 286(1):90–100. https://doi.org/10.1016/j.jcis.2005.01.007

Wu T, Yang G, Cao J, Zhengwei Xu, Jiang X (2022) Activation and adsorption mechanisms of methylene blue removal by porous biochar adsorbent derived from eggshell membrane. Chem Eng Res Des 188:330–341. https://doi.org/10.1016/j.cherd.2022.08.042

Xu Y, Luo G, He S, Deng F, Pang Q, Xu Y, Yao H (2019) Efficient removal of elemental mercury by magnetic chlorinated biochars derived from co-pyrolysis of Fe(NO$_3$)$_3$-laden wood and polyvinyl chloride waste. Fuel 239:982–990. https://doi.org/10.1016/j.fuel.2018.11.102

Zhang P, O'Connor D, Wang Y, Jiang L, Xia T, Wang L, Tsang DCW, Ok YS, Hou D (2020) A green biochar/iron oxide composite for methylene blue removal. J Hazard Mater 384:121286. https://doi.org/10.1016/j.jhazmat.2019.121286

Zhang H, Pap S, Taggart MA, Boyd KG, James NA, Gibb SW (2020) A review of the potential utilisation of plastic waste as adsorbent for removal of hazardous priority contaminants from aqueous. Environ Pollut 258:113698. https://doi.org/10.1016/j.envpol.2019.113698